Science Advances
AAAS

advances.sciencemag.org/cgi/content/full/4/10/eaat8797/DC1

Supplementary Materials for

Single-molecule observation of nucleotide induced conformational changes in basal SecA-ATP hydrolysis

Nagaraju Chada, Kanokporn Chattrakun, Brendan P. Marsh, Chunfeng Mao, Priya Bariya, Gavin M. King*

*Corresponding author. Email: kinggm@missouri.edu

Published 24 October 2018, *Sci. Adv.* **4**, eaat8797 (2018)
DOI: 10.1126/sciadv.aat8797

This PDF file includes:

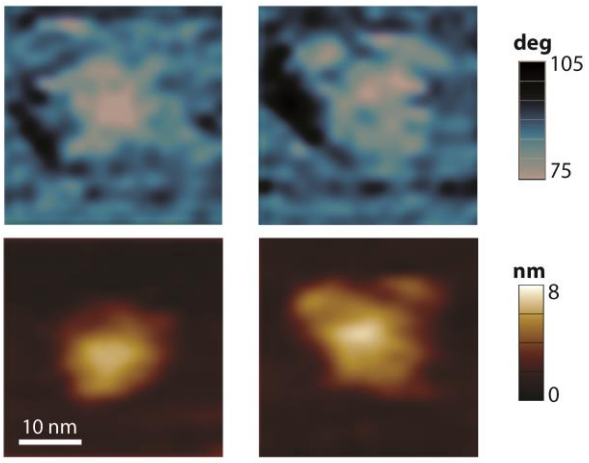

Fig. S1. Tapping mode phase imaging. Tapping mode phase images of SecA-WT are shown above the corresponding topographic images (data from Fig. 1F & G). Phase contrast is generally attributable to local changes in viscoelastic properties of the sample.

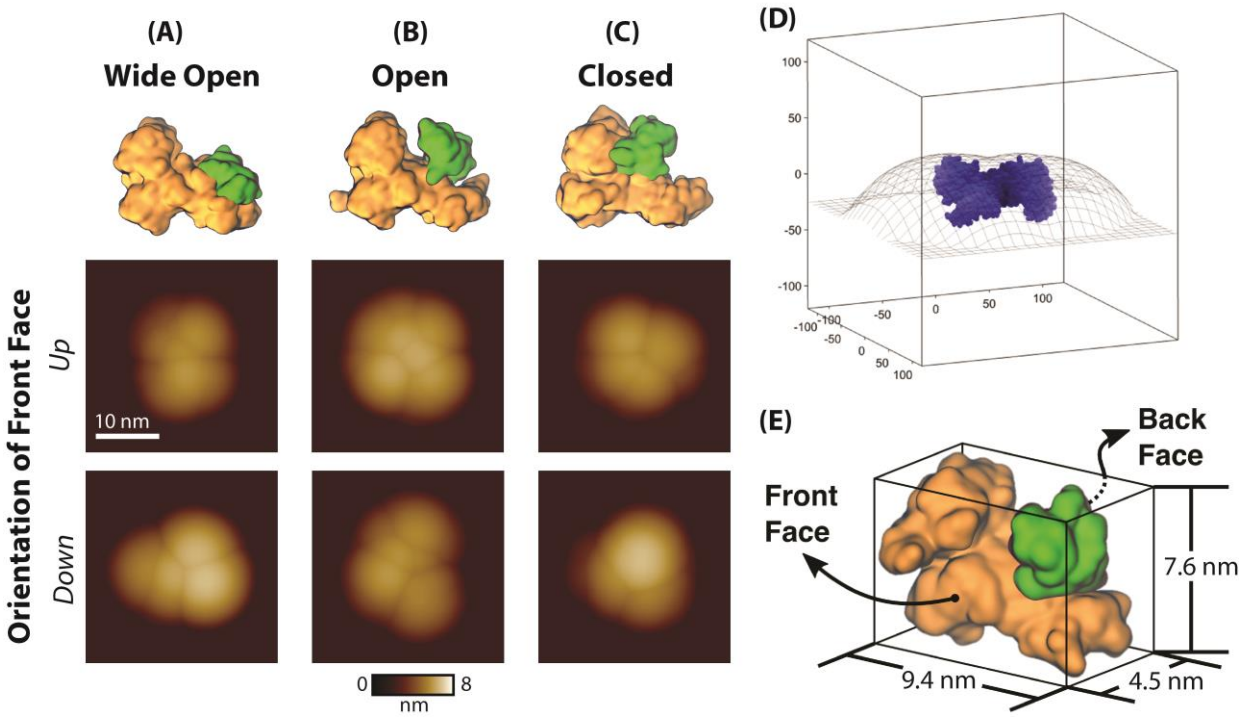

Fig. S2. Simulated AFM images and likely orientations of SecA on surface. Simulated AFM images were constructed from crystal structures and manufacturer nominal tip geometry (BL-AC40TS, Olympus; cone angle = 17.5°, tip radius = 8 nm). Column (**A**): PDB code 1M6N; (**B**): 1TF5; and (**C**): 3DIN. The protein binding domain is drawn in green. (**D**) Shows an example of the convoluted topographical surface (wire mesh) produced by morphological dilation. The protein is drawn in blue in this panel, the units are Å. (**E**) A rectangular volume with SecA inscribed defines two important faces of the molecule, the front and back face. We define the "up" orientation such that the front face of the molecule is in contact with the AFM tip. The "down" orientation is rotated by 180°, such that the front face of the molecule is in contact with the mica surface. We note that all of the experimental data exhibited prominent height peaks around 4.5 nm, consistent with either of these two orientations. All other orientations, without the large front or back face flush with the mica surface, would likely demonstrate height peaks >7 nm. However, significant sub-populations above 6 nm in height were not observed in the experimental data, suggesting a preference towards the up or down orientations. Hence, we focused our analysis on these two orientations. We note that in both the up and down orientation, the AFM tip can directly access and probe protein binding domain dynamics.

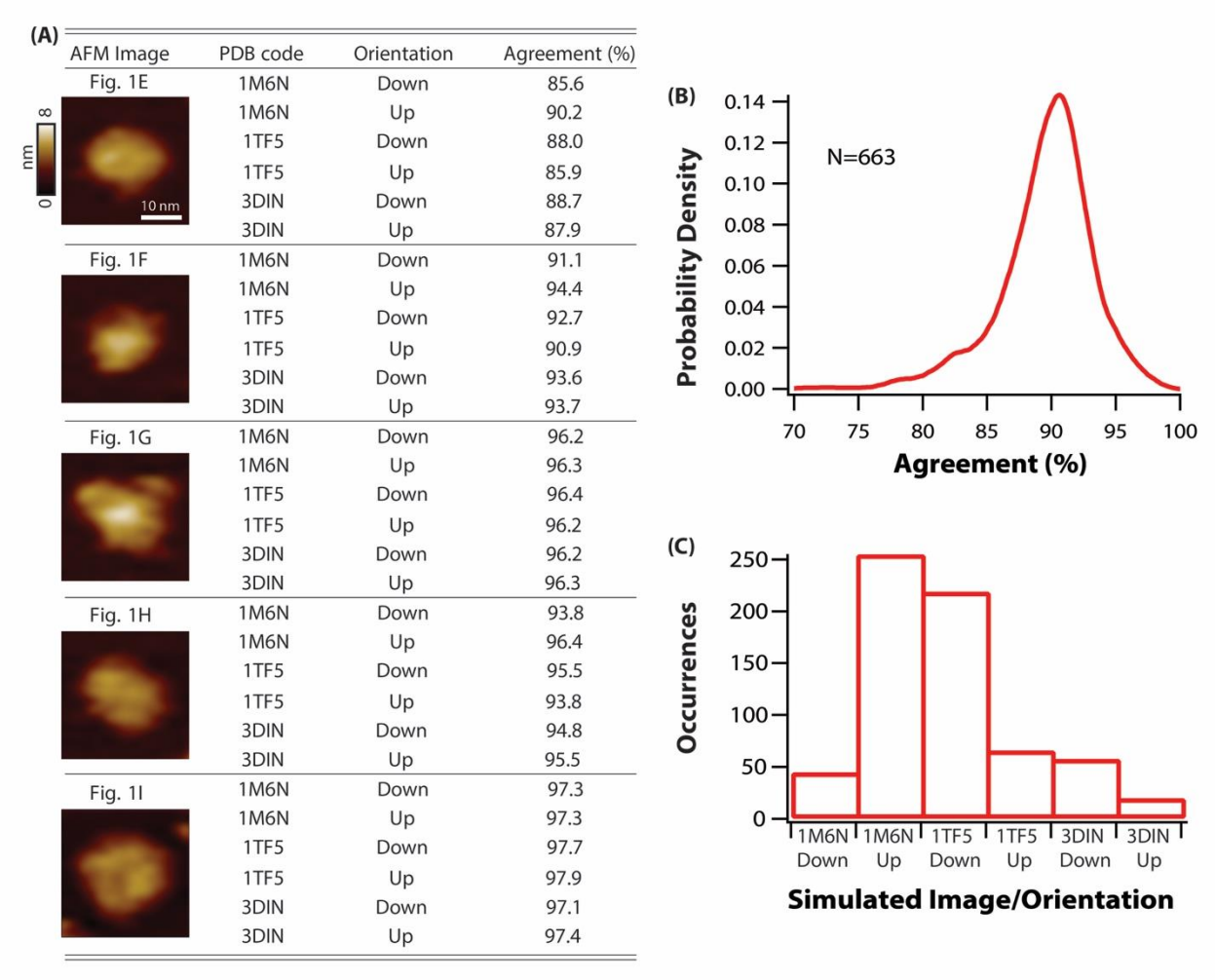

Fig. S3. AFM image data corroborate with simulations. (**A**) Comparison of five AFM images (Fig. 1E-I) to simulated images (fig. S2) based on crystal structures (protein data bank (PDB) codes listed) in the up and down orientations (defined in fig. S2). (**B**) Smoothed histogram showing the results of agreement analysis between a subset of $N = 663$ SecA-WT molecules in the apo condition and the same six simulated images. The data indicate that most of the AFM images are in good agreement (around 90%) with at least one of the simulated images. Here we plot only the maximum agreement between any of the six simulated images for each experimental image. (**C**) Shows the number of occurrences that a specific crystal/orientation achieved maximum agreement out of all six possible crystals/orientations. AFM data were most similar to simulated images of "wide open" conformation (1M6N) in the up orientation and "open" conformation (1TF5) in the down orientation.

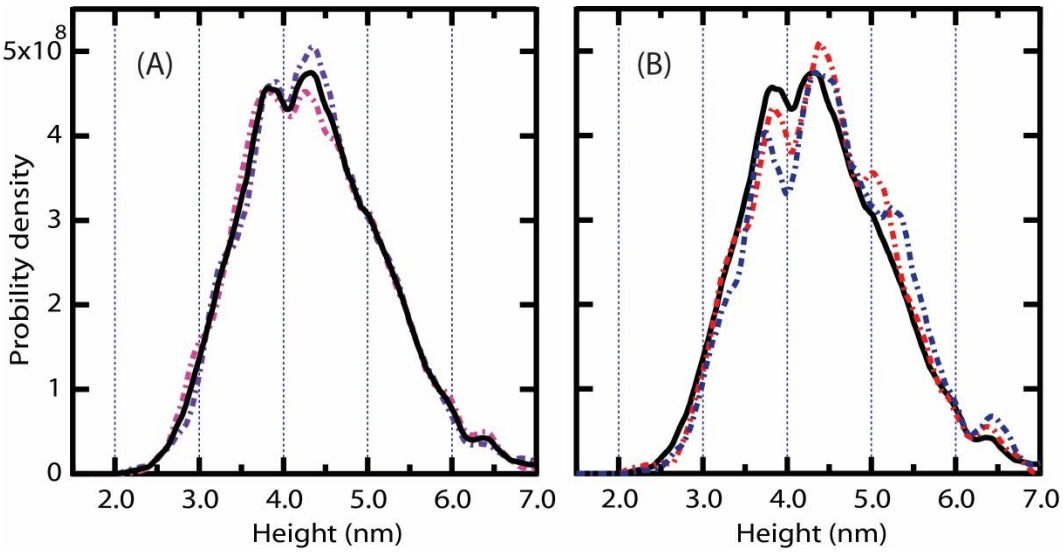

Fig. S4. Statistically robust subpopulations. (A) Height histogram of SecA-WT (black, *N* = *3726*) and two randomly culled subsets to *N*/2 (*dashed traces*) are shown. **(B)** Height histograms from two independent experiments (*dashed*) are compared to the summary histogram (*black*). This analysis verifies the presence of stable sub-populations.

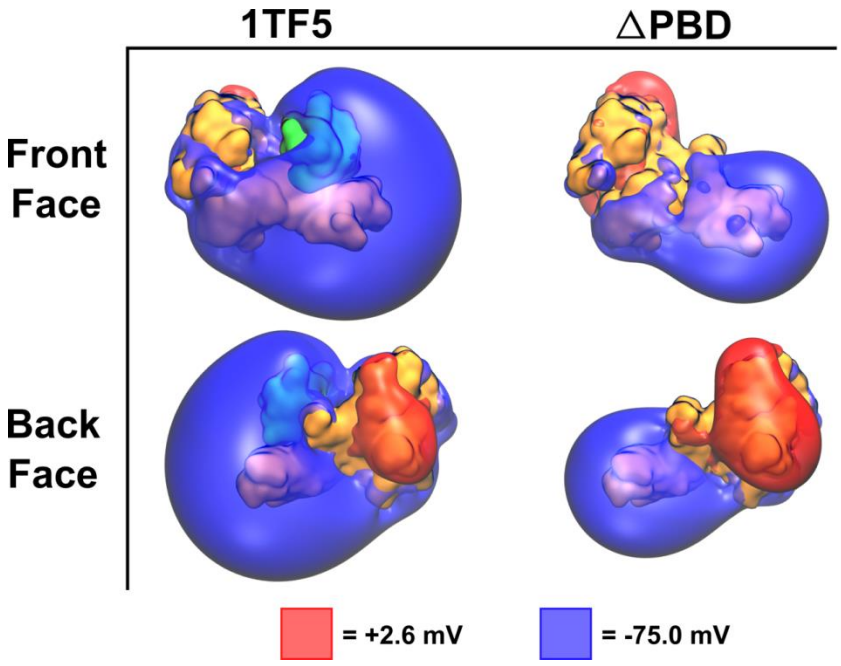

Fig. S5. Equipotential surfaces comparing the front and back faces of SecA. Surfaces of constant electrostatic potential at pH=7, generated from crystal structure 1TF5 and 1TF5 with the protein binding domain deleted (ΔPBD). Shown are views of the front and back faces of SecA (defined in fig. S2), which are likely to be oriented upwards towards the AFM tip during imaging. For both SecA species, the negative cloud on the front face is much larger in magnitude than the positive cloud on the back face; additionally both of the back faces have a slight di-polar nature. The data indicate that deleting the protein binding domain leads to an overall reduction of the negative potential, but asymmetry between the faces is preserved. This analysis suggests that the ΔPBD mutation is not likely to alter the overall orientation of SecA when adsorbed onto mica. This is consistent with our AFM observations.

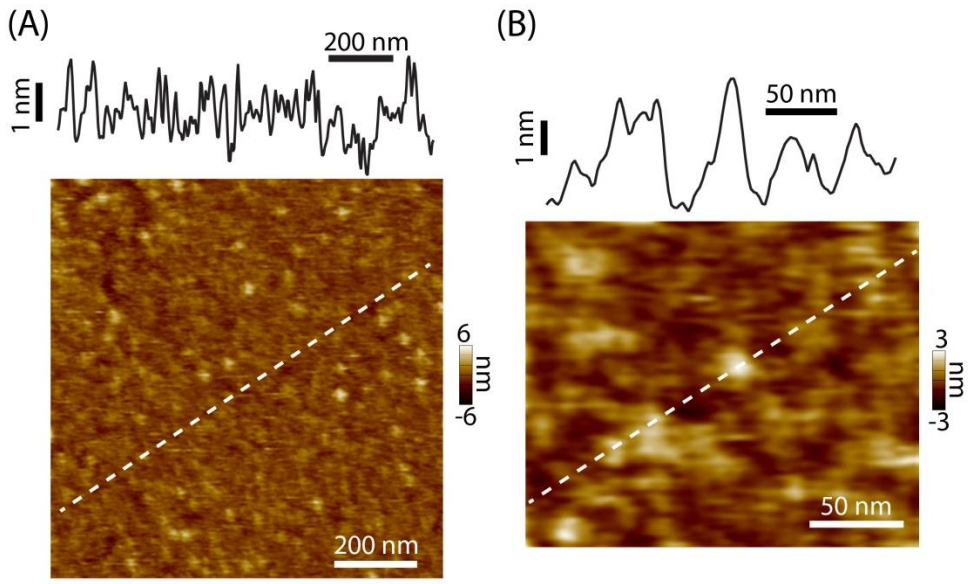

Fig. S6. Evaluation of molecular density of SecA prepared for surface-adsorbed ATPase activity assays. (**A**) AFM image of SecA prepared for surface-based ATPase measurements. Note, the incubation concentration used in this assay was 100-fold higher than that used for AFM analysis. Panel (**B**) shows a detailed view. Images were acquired in the presence of 3 mM ATP, line scans (*dashed*) are shown above each image. Under these conditions, the packing density of SecA prevents the tip from reaching the underlying mica in most areas. This observation suggests that the SecA has formed a continuous tightly-packed monolayer over the mica disk (radius ~5 mm). Based on the crystallographic dimensions of SecA and the likely orientation of the molecule on the surface (fig. S2) we estimate a per-molecule area footprint of approximately 4800 $Å^2$ and hence, calculate there to be about 3×10^{-12} mol SecA on the mica. We note that this per-molecule area is smaller than the AFM image area because it does not account for tip convolution.

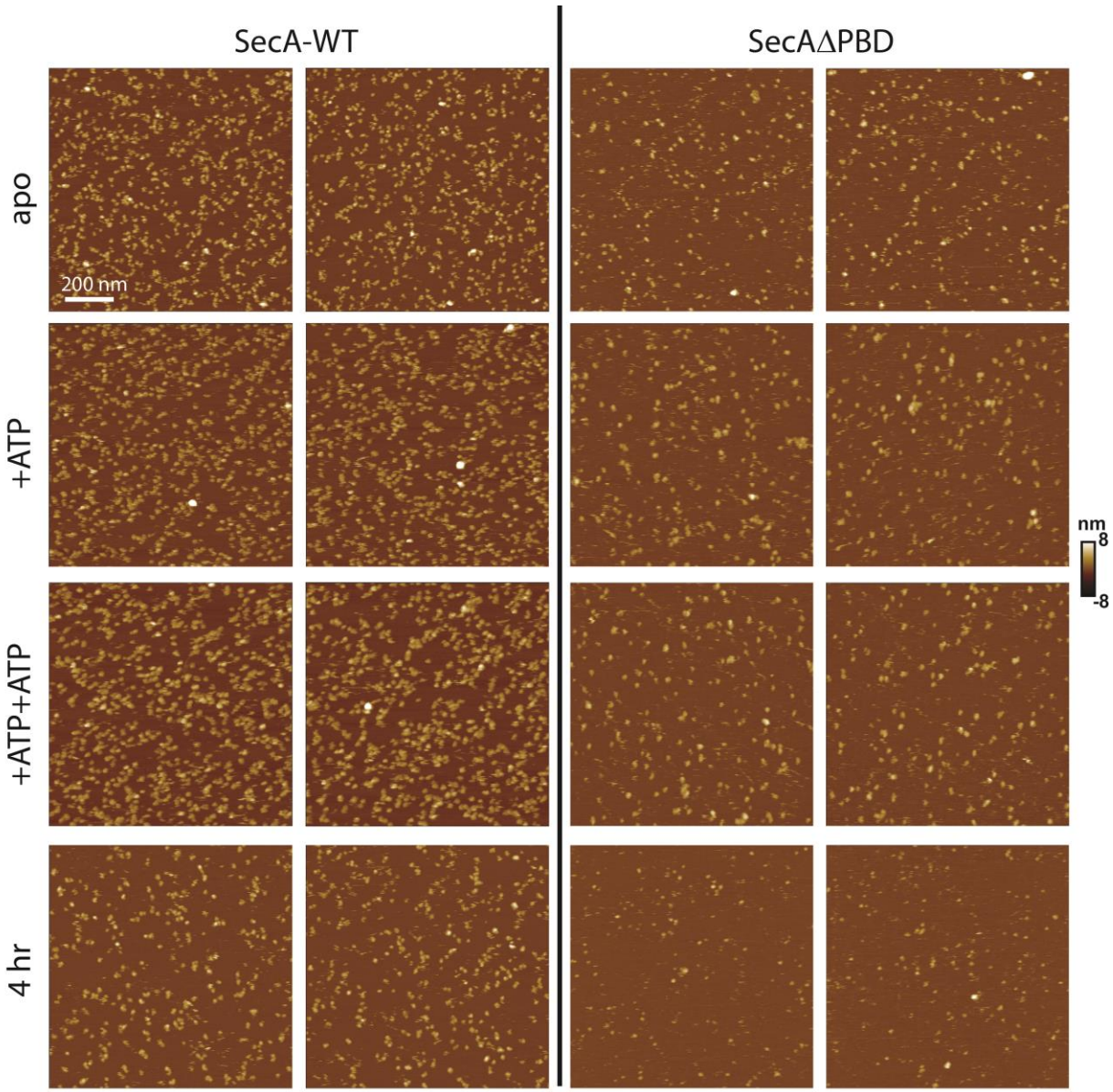

Fig. S7. Representative images of SecA-WT and SecAΔPBD subject to different conditions. apo = not exposed to any nucleotide after purification; +ATP = pre-incubated with 100 μM ATP for 15 min prior to deposition on mica and then imaged in the absence of ATP; +ATP+ATP = pre-incubated with 100 μM ATP in solution for 15 min and then imaged with 100 μM ATP in the imaging buffer; and 4 hr = pre-incubated with 100 μM ATP in solution for 4 hours and then imaged in the absence of ATP in the imaging buffer.

Table S1. Statistics of SecA-WT (WT) and SecAΔPBD (ΔPBD) area distributions in the following conditions. (*i*) apo = not exposed to any nucleotide after purification; (*ii*) +ATP = pre-incubated with 100 μM ATP for 15 min prior to deposition on mica and then imaged in the absence of ATP; (*iii*) +ATP+ATP = pre-incubated with 100 μM ATP in solution for 15 min and then imaged with 100 μM ATP in the imaging buffer; and (*iv*) 4 hr = pre-incubated with 100 μM ATP in solution for 4 hours and then imaged in the absence of ATP in the imaging buffer. We show the number of features included in the analysis *N*; the mean area footprint ± standard error of the mean; as well as the peak area ± error, as determined via the most populated bin in the area histogram ± the bin width.

Assay	*N* - WT	Mean Area WT [nm^2]	Peak Area WT [nm^2]	*N* - ΔPBD	Mean Area ΔPBD [nm^2]	Peak Area ΔPBD [nm^2]
(i) apo	3726	480 ± 6	200 ± 10	4009	380 ± 4	230 ± 10
(ii) +ATP	3376	650 ± 9	270 ± 10	1907	580 ± 9	230 ± 10
(iii) +ATP+ATP	2437	940 ± 17	300 ± 10	1458	570 ± 9	300 ± 10
(iv) 4 hr	2448	450 ± 6	280 ± 10	1061	330 ± 8	235 ± 10

Table S2. Mean height (±SEM) and FWHM of the SecA-WT and the SecAΔPBD mutant height distributions in different conditions.

ATP Assay	*N* - WT	Mean Height WT [Å]	FWHM WT [Å]	*N* - ΔPBD	Mean Height ΔPBD [Å]	FWHM ΔPBD [Å]
(i) apo	3726	44 ± 0.2	20	4009	42 ± 0.2	17
(ii) +ATP	3376	41 ± 0.2	21	1907	36 ± 0.2	15
(iii) +ATP+ATP	2437	44 ± 0.3	23	1458	39 ± 0.3	15
(iv) 4 hr	2448	38 ± 0.2	16	1061	34 ± 0.3	14

Table S3. Statistics of the SecA-WT and SecAΔPBD area distributions after exposure to ADP or ADP-AlF$_3$. We show the number of features included in the analysis *N*; the mean area footprint ± standard error of the mean; as well as the peak area ± error, as determined via the most populated bin in the area histogram ± the bin width.

Nucleotide	*N*-WT	Mean Area WT [nm^2]	Peak Area WT [nm^2]	*N*-ΔPBD	Mean Area ΔPBD [nm^2]	Peak Area ΔPBD [nm^2]
ADP	6428	420 ± 4	220 ± 10	3104	390 ± 5	220 ± 10
ADP-AlF$_3$	4590	360 ± 4	235 ± 10	2159	320 ± 6	220 ± 10

Table S4. Mean height (±SEM) and FWHM of the SecA-WT and the SecAΔPBD mutant distributions exposed to ADP and ADP-AlF$_3$.

Nucleotide	*N* - WT	Mean Height WT [Å]	FWHM WT [Å]	*N* - ΔPBD	Mean Height ΔPBD [Å]	FWHM ΔPBD [Å]
ADP	6428	42 ± 0.2	18	3104	42 ± 0.2	17
ADP-AlF$_3$	4590	40 ± 0.2	15	2159	37 ± 0.3	16

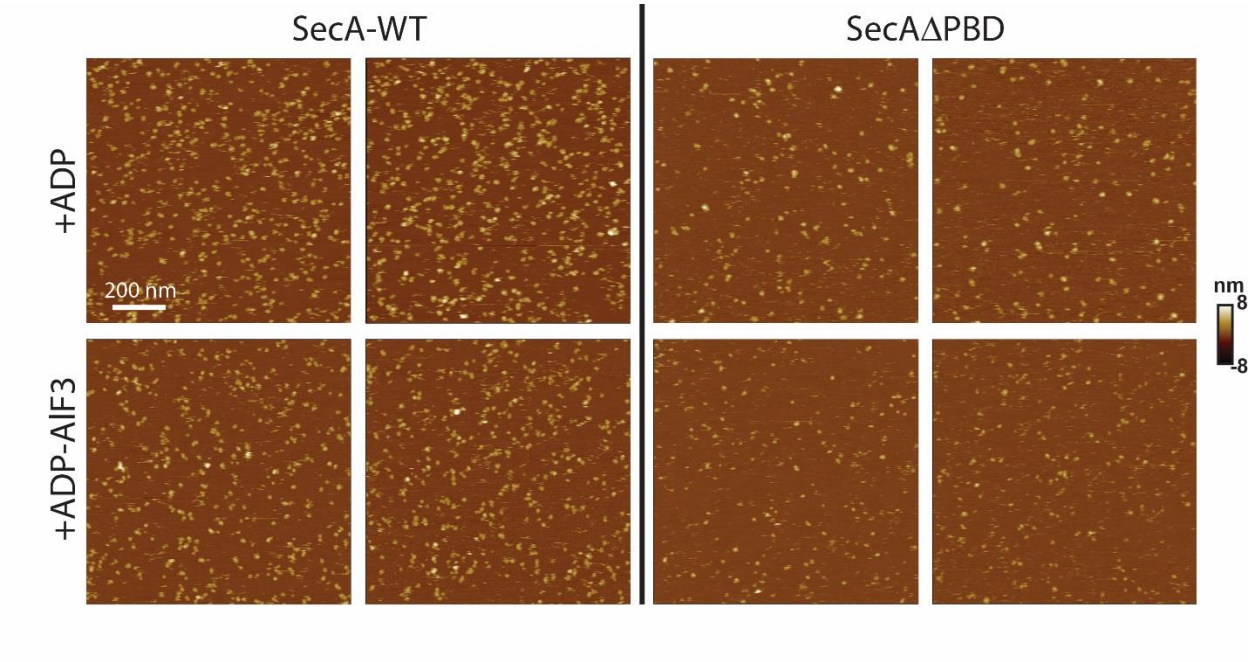

Fig. S8. Representative images of SecA-WT and SecAΔPBD exposed to different nucleotides. Enzymes were exposed to ADP or ADP-AlF_3 for 15 mins prior to imaging, and then imaged in the absence of nucleotides.

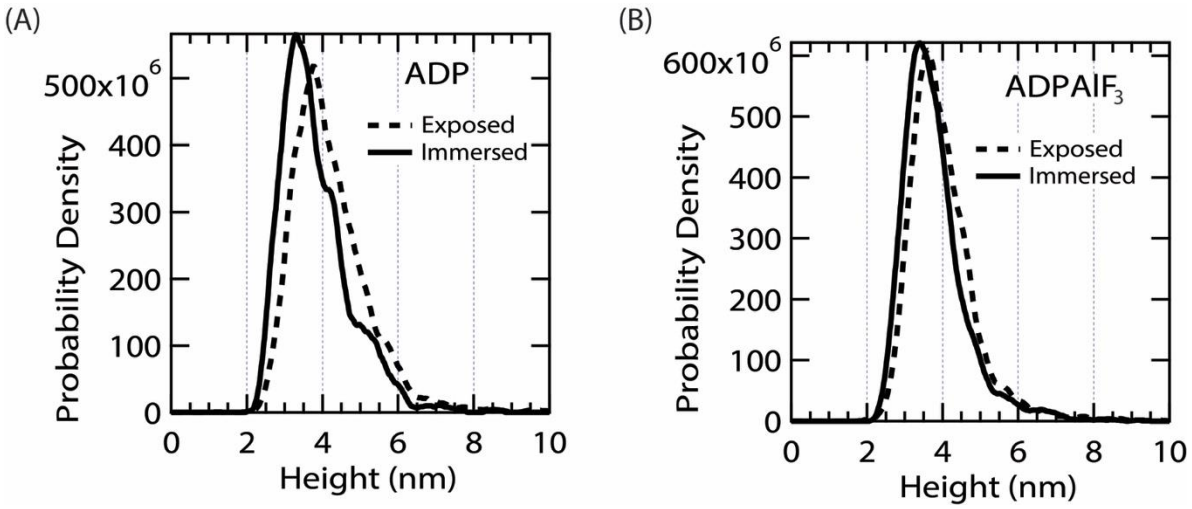

Fig. S9. Height histograms of SecA immersed in and exposed to nonhydrolyzable nucleotides. (**A**) Comparison of height histograms for SecA-WT when imaged in (*solid line*, N = 1090) or just after exposure to (*dashed*, N = 6428) ADP. (**B**) Analogous data for ADP-AlF_3 (Immersed: N = 1561; Exposed: N = 4590). These data indicate that the presence of the nucleotides in the AFM imaging buffer results in slight downward height shifts of 4 or 2 Å, for ADP and ADP-AlF_3, respectively.

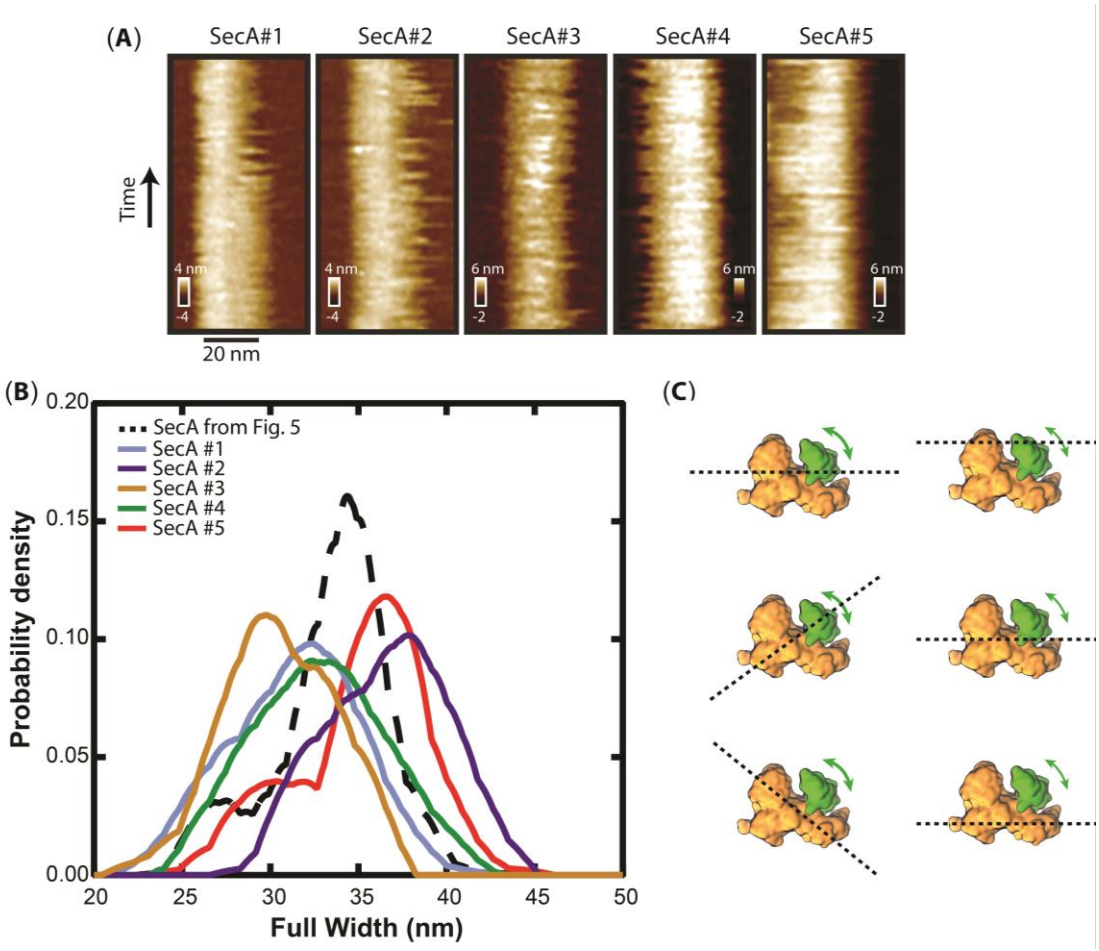

Fig. S10. Additional kymograph data. (**A**) Kymograph segments (temporal duration 12.4 s) of five distinct SecA-WT molecules in the presence of saturating ATP. (**B**) Histograms showing the full width distribution of each molecule. The number of line scans evaluated: N = 125, 64, 64, 75, and 75, for SecA#1–5, respectively. Data from Fig. 5 is carried over for reference (dashed). (**C**) Cartoons (drawn with the front face "up" orientation, defined in fig. S2) demonstrate variations due to angular (left column) and translational (right column) offsets on the resulting one-dimensional scanning measurements (*dashed lines*). Certain scan trajectories are better suited to observe protein binding domain (*green*) dynamics. Despite variations, evidence of at least two states ('compact' and 'extended') can be observed in the data.